

# Experimental and Theoretical Studies of Charge Delocalization in Biruthenium–Alkynyl Complexes Bridged by Thiophenes

Ya-Ping Ou, Jianlong Xia, Jing Zhang, Meng Xu, Jun Yin, Guang-Ao Yu, and Sheng Hua Liu\*<sup>[a]</sup>

**Abstract:** A series of binuclear ruthenium–alkynyl complexes that are bridged by thiophene groups (thiophene, bi-thiophene, and terthiophene) have been synthesized. All of these complexes have been well-characterized by NMR spectroscopy, X-ray diffraction, and elemental analysis. The electronic properties of these complexes have been examined by using cyclic voltammetry, UV/Vis/NIR and IR spectroscopy,

electron paramagnetic resonance (EPR) spectroscopy, and density functional theory (DFT) calculations. Electrochemical results showed that the potential difference ( $\Delta E$ ) and comproportionation constant ( $K_c$ ) decreased with

increasing size of the thiophene bridging unit. The UV/Vis/NIR spectra and TDDFT calculations of the monocations indicated that the NIR transitions displayed aromatic bridging character. EPR studies of the mono-oxidized radical species further demonstrated that the unpaired electron/hole was delocalized over both metals and the bridging ligand and established significant participation in the ligand oxidation.

**Keywords:** bridging ligands • radicals • redox chemistry • ruthenium • thiophenes

## Introduction

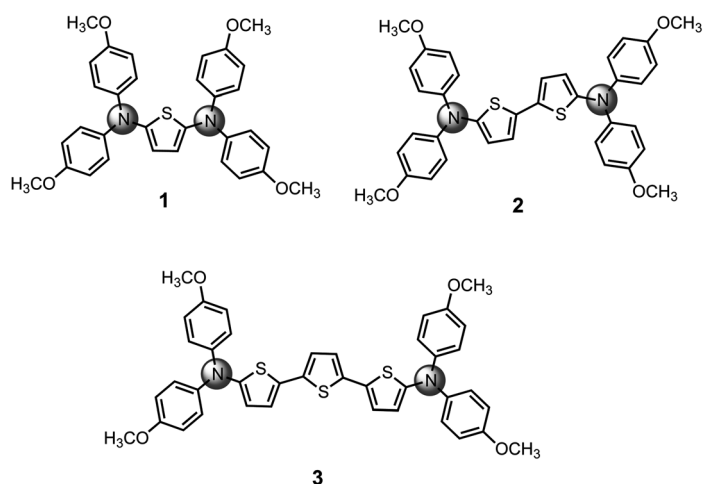
Recently, ligand-bridged bimetallic complexes<sup>[1]</sup> have attracted extensive interest because of their potential applications in many fields, such as solar cells,<sup>[2]</sup> electron-transfer reactions,<sup>[3]</sup> and molecular electronic devices.<sup>[4]</sup> Since the first synthesis of binuclear ruthenium complexes [Ru(NH<sub>3</sub>)<sub>5</sub>](pyrazine)[Ru(NH<sub>3</sub>)<sub>5</sub>]<sup>5+</sup>, named as the Creutz–Taube ion,<sup>[5]</sup> continuous investigations have involved using [(L<sub>n</sub>M)(μ-bridge)(ML<sub>n</sub>)]-type<sup>[6–8]</sup> bimetallic complex as the precursor for mixed-valence systems, which are linked by a conjugated bridging ligand. Typically, these bimetallic complexes exhibit strong electronic communication between the two redox-active metal ends, which enable their potential use as organometallic molecular wires. The degree of electronic communication between the two metal centers depends on many factors, including the bridging ligands, the ancillary ligands, and the intrinsic properties of the transition metals.<sup>[1c]</sup> It has been well-established that the bridging ligands play an important role in tuning the electronic properties of the final binuclear complexes; thus, the synthesis of these compounds with various bridging ligands has attracted significant interest from organic chemists. The most-recent research on bi-

metallic complexes has been devoted to determining the redox processes of these complexes, that is, either “ligand redox non-innocence” or “metal-dominated oxidation” (classical mixed-valence concept).<sup>[8b,d,9]</sup> A combination of electrochemical and spectroscopic techniques has been used to accurately determine the redox processes of the bimetallic complexes. In addition, theoretical calculations are powerful supplements to the experimental data. Studies on the effect of various organic ligands on the redox processes of bimetallic complexes will help to rationalize the design of new transition-metal complexes for molecular electronic devices.

Oligothiophenes are excellent electron-donating materials and have been widely used as hole-transport materials in several types of optical and electronic devices.<sup>[10]</sup> Thiophene has been widely used as a starting material for the synthesis of oligothiophene derivatives.<sup>[11]</sup> Therefore, this series of derivatives provides abundant resources for research into organic semiconductor materials<sup>[12]</sup> and molecular electronic devices.<sup>[13]</sup> Recently, oligothiophene derivatives have also been used as bridging ligands for organic and inorganic mixed-valence systems<sup>[14]</sup> and the electron-transfer properties of these systems have also been investigated. In a previous work, Wenger and co-workers synthesized a homologous series of  $\alpha,\alpha'$ -bis(diphenylamino)-substituted thiophene derivatives (Scheme 1) and studied their electronic coupling properties.<sup>[15]</sup> In 2007, Chen's group reported a series of binuclear ruthenium complexes that were connected by bis-(ethynyl)oligothiophenes and investigated their electrochemical and UV/Vis/NIR spectroscopic properties in different valence states.<sup>[16]</sup> With these reports in mind, herein, we report the synthesis and characterization of a series of homobimetallic ruthenium–alkynyl complexes that are bridged

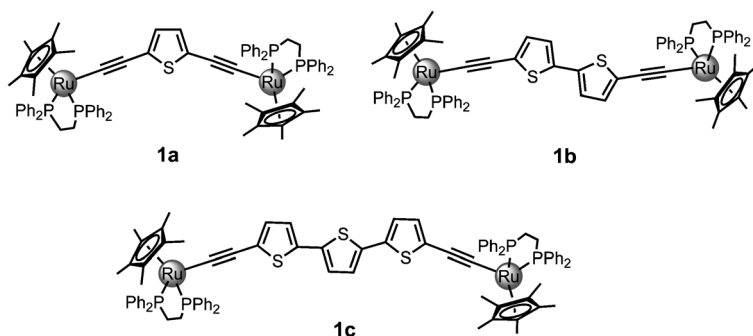
[a] Y.-P. Ou, J. Xia, J. Zhang, M. Xu, Prof. Dr. J. Yin, Prof. Dr. G.-A. Yu, Prof. Dr. S. H. Liu  
Key Laboratory of Pesticide and Chemical Biology  
Ministry of Education  
College of Chemistry, Central China Normal University  
152 Luoyu Road, Wuhan, Hubei 430079 (China)  
Fax: (+86) 27-67867725  
E-mail: chshliu@mail.ccnu.edu.cn

Supporting information for this article is available on the WWW under <http://dx.doi.org/10.1002/asia.201300419>.

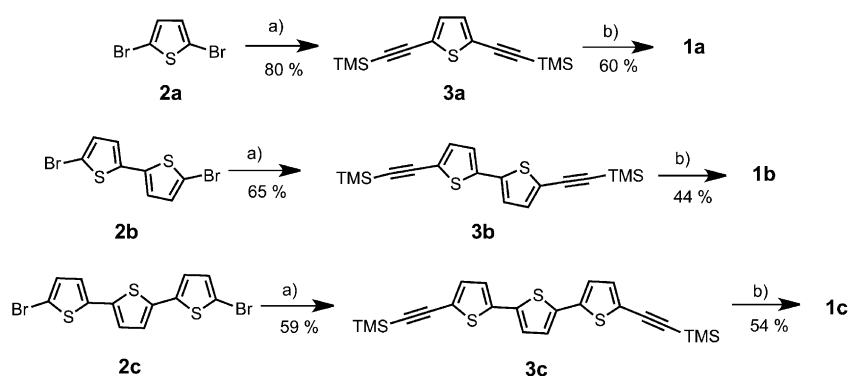


Scheme 1.  $\alpha,\alpha'$ -Bis(diphenylamino)-substituted thiophene derivatives.

by oligothiophenes (Scheme 2). These bimetallic complexes have been fully characterized by using NMR spectroscopy, X-ray diffraction, and elemental analysis. The electronic properties of these complexes and their redox behaviors have been investigated by using electrochemistry, IR, UV/Vis/NIR, and EPR spectroscopy, and by computational studies.



Scheme 2. Oligothiophene-based bimetallic ruthenium complexes **1a–1c**.



Scheme 3. Reagents and conditions: a) TMSA,  $[\text{Pd}(\text{PPh}_3)_4]$ , CuI, THF/ $\text{Et}_3\text{N}$  or  $(i\text{Pr})_2\text{NH}$ ; b)  $[\text{RuCl}(\text{dppe})\text{Cp}^*]$ , KF, MeOH/THF. TMSA = trimethylsilylacetylene, dppe = 1,2-bis(diphenylphosphino)ethane,  $\text{Cp}^*$  = 1,2,3,4,5-pentamethylcyclopentadiene.

## Results and Discussion

### Synthesis and Characterization

The general synthetic route for the preparation of oligothiophene-based bimetallic ruthenium–acetylide complexes **1a–1c** is shown in Scheme 3. Compounds **3a–3c** were obtained in 59–80% yield by using a Pd/Cu-catalyzed Sonogashira coupling reaction between 2,5-dibromothiophene, 5,5'-dibromo-2,2'-bithiophene, and 5,5'-dibromo-2,2':5',2''-terthiophene, respectively, and (trimethylsilyl)acetylene. Subsequently, TMS-protected compounds **3a–3c** were deprotected with KF and reacted in situ with  $[\text{RuCl}(\text{dppe})\text{Cp}^*]$  at 60 °C.<sup>[17]</sup> Target complexes **1a–1c** were obtained by filtration and characterized by using conventional spectroscopic methods. However, the  $^{13}\text{C}$  NMR spectrum of complex **1b** could not be obtained, owing to its poor solubility. In the  $^1\text{H}$  NMR spectrum, the proton signals of the thiophenes were overlapped with the proton signals of the dppe ligand. The  $^{13}\text{C}$  NMR resonances of typical Ru–C moieties in compounds **1a** and **1c** were observed at  $\delta = 123.65$  and 125.10 ppm, respectively. The  $^{31}\text{P}$  NMR resonances of complexes **1a–1c** were gradually shifted from  $\delta = 78.01$  to 79.93 ppm with increasing bridge length. The IR spectra of complexes **1a–1c**, which were recorded in both the solid and solution states, displayed  $\nu(\text{C}=\text{C})$  signals at about 2064, 2056, and 2046  $\text{cm}^{-1}$ , respectively.

The structure of compound **1c** (Figure 1) was confirmed by single-crystal X-ray analysis (Table 1). Details of the data collection and refinement are presented in the Supporting Information, Table S1; selected bond lengths and angles in DFT-optimized structures  $[\mathbf{1a-H}]^{n+}$  ( $n=0, 1, 2$ ) and  $[\mathbf{1b-H}]^{n+}$  ( $n=0, 1, 2$ ) are provided in the Supporting Information, Tables S2 and S3, respectively. The extension “–H” indicates that the  $\eta\text{-C}_5\text{Me}_5$  and dppe ligands in compounds **1a–1c** were replaced by  $\eta\text{-C}_5\text{H}_5$  and two  $\text{PH}_3$  ligands (see below). According to the crystal structure of complex **1c** (Figure 1), this molecule exhibits pseudo-octahedral geometry, similar to that observed in closely related compounds.<sup>[18]</sup> The three thiophene rings are not coplanar, but their dihedral angles are less than 20°. The Ru1–Ru2 distance in complex **1c** is 18.972 Å, as shown in Table 1; the Ru1–C37 bond length is 1.988 Å and the length of the

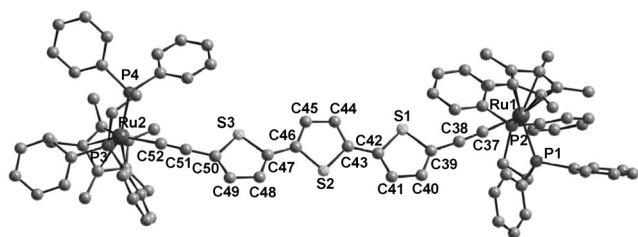


Figure 1. Molecular structure of compound **1c**, which shows the atom-labelling scheme; hydrogen atoms are omitted for clarity.

Table 1. Selected bond lengths [Å] and angles [°] in the crystal structure of compound **1c** and in DFT-optimized structures [**1c-H**]<sup>n<M+></sup> (*n* = 0, 1, 2).

	<b>1c</b>	[ <b>1c-H</b> ]	[ <b>1c-H</b> ] <sup>+</sup>	[ <b>1c-H</b> ] <sup>2+</sup>
Ru1–C37	1.988	2.010	1.972	1.932
Ru1–P1,2	2.272,	2.281,	2.297,	2.317,
	2.257	2.280	2.298	2.318
C37–C38	1.219	1.230	1.240	1.252
C38–C39	1.422	1.400	1.377	1.356
C39–C40	1.363	1.386	1.409	1.434
C40–C41	1.415	1.417	1.392	1.371
C41–C42	1.363	1.385	1.406	1.429
C42–S1	1.728	1.756	1.759	1.765
S1–C39	1.740	1.766	1.766	1.767
C42–C43	1.463	1.439	1.412	1.387
C43–C44	1.342	1.384	1.406	1.431
C44–C45	1.386	1.417	1.392	1.370
C43–S2	1.714	1.759	1.760	1.764
P1–Ru1–P2	83.41	93.18	92.66	91.52
Ru1–C37–C38	177.50	179.00	178.46	177.96
C37–C38–C39	175.66	178.50	178.66	178.64

triple bond C37–C38 is 1.219 Å. Bond angles Ru1–C37–C38 and C37–C38–C39 are 177.50° and 175.66°, respectively, which are both near to 180°. Oxidation of model complex [**1c-H**] into [**1c-H**]<sup>2+</sup> caused an elongation of the C37–C38 and Ru–P1,2 bonds, together with a shortening of the Ru1–C37 bond.

### Electrochemical Properties

The values of  $\Delta E$  ( $\Delta E = E_{1/2}^2 - E_{1/2}^1$ ) and  $K_c$  ( $K_c = e^{\Delta E F / (RT)}$ ),<sup>[19–22]</sup> as measured by using cyclic voltammetric (CV), are used to determine the thermodynamic stability of the oxidized states (or mixed-valence species). The electrochemical properties of complexes **1a–1c** were also investigated by using cyclic voltammetry and square-wave voltammetry (SWV). CV at different scan rates and SWV at 100 mV s<sup>-1</sup> with [NBu<sub>4</sub>]PF<sub>6</sub> (0.1 M) as a supporting electrolyte in CH<sub>2</sub>Cl<sub>2</sub> showed that complexes **1a** and **1b** underwent two consecutive one-electron-oxidation processes, whereas complex **1c** showed no apparent peak separation and displayed a one-step redox process within the electrochemical window of the solvent (Figure 2). Detailed electrochemical data are listed in Table 2. As shown in Table 2, with increasing length of the bridging thiophene units, complexes **1a–1c** exhibited sequentially increasing oxidation potentials ( $E_{1/2}(1)$ ), whereas

the potential difference with the second oxidation potential ( $E_{1/2}(2)$ ) for compounds **1a** and **1b** is inconspicuous. Complex **1c** shows no detectable  $E_{1/2}(2)$  potential within the electrochemical window. The potential difference ( $\Delta E$ ) and comproportionation constant ( $K_c$ ) become smaller with increasing length of the bridging ligands. Complexes **1a** and **1b** have  $\Delta E$  values of 320 and 137 mV and  $K_c = 2.25 \times 10^5$  and 207, respectively. Complex **1c** shows no detectable  $\Delta E$  and  $K_c$  values under the same conditions. These results indicate that the stability of the mixed-valence states is also highly dependent on the length of the bridging ligands. Furthermore, the rather substantial comproportionation constants ( $K_c$ ) of complexes **1a** and **1b** indicate that radical species [**1a**]<sup>+</sup> and [**1b**]<sup>+</sup> should be stable enough for spectroscopic characterization (see below).

### IR Spectroscopy

IR spectroscopy is widely used to investigate the changes in the stretching frequencies of complexes that contain IR-active functional groups (C≡C and CO) in different redox states.<sup>[23,24]</sup> These strong, characteristic absorptions provide suitable spectroscopic probes for studying the effect of oxidation on the structural change of the ligand, as brought about by using chemical methods. In addition, the changes in C≡C and CO stretching frequencies are often helpful for understanding the degree of charge delocalization in mixed-valence systems.<sup>[23]</sup>

Electrochemical studies revealed that both the first and second oxidation potentials of these complexes were negative. Furthermore, from a literature search of chemical oxidizing agents,<sup>[25]</sup> we found that ferrocenium hexafluorophosphate has been widely used as a mild oxidizing agent to oxidize biruthenium complexes into isolable mono- and dications.<sup>[16,26]</sup> Herein, we report the oxidation titration of complexes **1a–1c** by using ferrocenium hexafluorophosphate as an oxidant, after which the in situ generated radical species were characterized by using IR spectroscopy, without isolation. The characteristic  $\nu(\text{C}\equiv\text{C})$  vibrational frequencies of different redox states are listed in Table 3. The  $\nu(\text{C}\equiv\text{C})$  bands of neutral complexes **1a–1c** appeared at 2056, 2055, and 2046 cm<sup>-1</sup>, respectively. The mono-oxidized species were formed after adding 1.0 equivalent of the oxidant. New C≡C vibrations appeared in the IR spectra of cations [**1b**]<sup>+</sup> ( $\nu(\text{C}\equiv\text{C})$ : 1982, 1933 cm<sup>-1</sup>;  $\Delta\nu(\text{C}\equiv\text{C}) = 49$  cm<sup>-1</sup>) and [**1c**]<sup>+</sup> ( $\nu(\text{C}\equiv\text{C})$ : 2007, 1920 cm<sup>-1</sup>;  $\Delta\nu(\text{C}\equiv\text{C}) = 87$  cm<sup>-1</sup>); both spectra displayed two  $\nu(\text{C}\equiv\text{C})$  bands (Figure 3B,C). This result is similar the reported spectra of diethynyl-bridged complexes [1,4-{Cp\*(dppe)RuC≡C}<sub>2</sub>C<sub>6</sub>H<sub>4</sub>]<sup>[8b,27]</sup> and [1,3-{Cp\*(dppe)RuC≡C}<sub>2</sub>C<sub>6</sub>H<sub>4</sub>]<sup>[23]</sup>. This result indicates that the odd electron is not fully delocalized over the whole framework on the IR timescale ( $\times 10^{-13}$  s<sup>-1</sup>). Complex [**1a**]<sup>+</sup> showed a very strong, single  $\nu(\text{C}\equiv\text{C})$  band absorption at 1961 cm<sup>-1</sup>, thus indicating the formation of resonance structures between the thiophene ring and two C≡C bonds, which suggested that strong participation of the bridge in the first oxidation process. Continuing the one-electron oxidation into

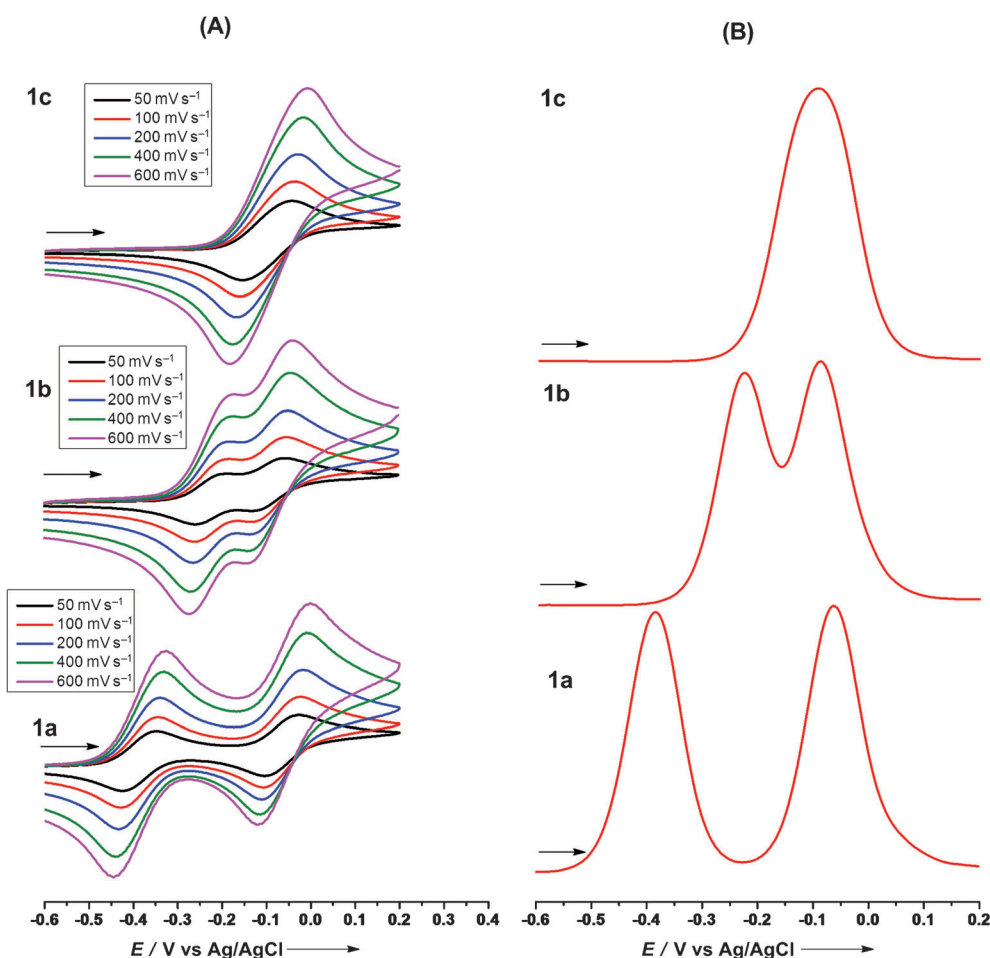


Figure 2. A) CVs of complexes **1a–1c** in  $\text{CH}_2\text{Cl}_2/\text{Bu}_4\text{NPF}_6$  at different scan rates (0.05, 0.1, 0.2, 0.4, and 0.6  $\text{V s}^{-1}$ ). B) SWVs of complexes **1a–1c** (scan rate: 0.1  $\text{V s}^{-1}$ ,  $f = 10$  Hz).

Table 2. Electrochemical data for complexes **1a–1c**.<sup>[a]</sup>

Complex	$E_{1/2}(1)$ [V]	$E_{1/2}(2)$ [V]	$\Delta E$ [mV] <sup>[b]</sup>	$K_c$ <sup>[c]</sup>
<b>1a</b>	-0.387	-0.064	320	$2.25 \times 10^5$
<b>1b</b>	-0.224	-0.087	137	207
<b>1c</b>	-0.092	-	-	-

[a] Potentials are versus the  $\text{Fc}^+/\text{Fc}$  couple from single-scan CVs that were recorded at 298 K in 0.1 M  $(\text{Bu}_4\text{N})(\text{PF}_6)$  in  $\text{CH}_2\text{Cl}_2$ . Additional oxidation waves of the thienyl moiety were observed at higher potentials but were not examined further. [b]  $\Delta E = E_{1/2}(2) - E_{1/2}(1)$  denotes the potential difference between the two redox processes. [c] The comproportionation constants,  $K_c$ , were calculated according to the formula  $K_c = \exp(\Delta E/25.69)$  at 298 K.

Table 3. Summary of the  $\nu(\text{C}\equiv\text{C})$  vibrational frequencies [ $\text{cm}^{-1}$ ] in the IR spectra of complexes  $[\mathbf{1a-1c}]^{n<M+>}$  ( $n=0, 1, 2$ ), as determined by chemical oxidation in the presence of various equivalents of the oxidant (0, 1.0, and 2.0 equiv).

Complex	$n=0$	$n=1$	$n=2$
<b>1a</b>	2056 (m)	1961 (vs)	1914 (m)
<b>1b</b>	2055 (m)	1982 (m), 1933 (vs)	1909 (m)
<b>1c</b>	2046 (m)	2007 (m), 1920 (s)	1971 (w), 1917 (m)

$\text{Ru}^{\text{III/III}}$  species with the addition of 2.0 equivalents of ferrocenium hexafluorophosphate, further shifts were found for complexes  $[\mathbf{1a}]^{2+}$  (1914  $\text{cm}^{-1}$ ),  $[\mathbf{1b}]^{2+}$  (1909  $\text{cm}^{-1}$ ), and  $[\mathbf{1c}]^{2+}$  (1971, 1917  $\text{cm}^{-1}$ ). Complexes  $[\mathbf{1a}]^{2+}$  and  $[\mathbf{1b}]^{2+}$  exhibited single medium-to-strong  $\nu(\text{C}\equiv\text{C})$  bands; this result indicated a highly symmetric distribution of charge in the dication.<sup>[36]</sup> Surprisingly, two weak  $\nu(\text{C}\equiv\text{C})$  bands were observed in the spectrum of complex  $[\mathbf{1c}]^{2+}$ , which could originate from the contribution of the bridge ligand in the oxidation process.

### UV/Vis/NIR Spectroscopy

To further probe the electronic delocalization of complexes **1a–1c**, the changes in their UV/Vis/NIR absorption spectra were monitored upon the gradual addition of ferrocenium hexafluorophosphate (Figure 4 and the Supporting Information, Figures S1 and S2). The electronic absorption spectroscopic data of compounds **1a–1c** in various oxidation states are listed in Table 4. When solutions of complexes **1a–1c** in  $\text{CH}_2\text{Cl}_2$  were treated with incremental amounts of ferrocenium hexafluorophosphate, from 0 to 1.0 equivalents, intense  $\pi-\pi^*$  transitions were observed in the UV-light region (250–

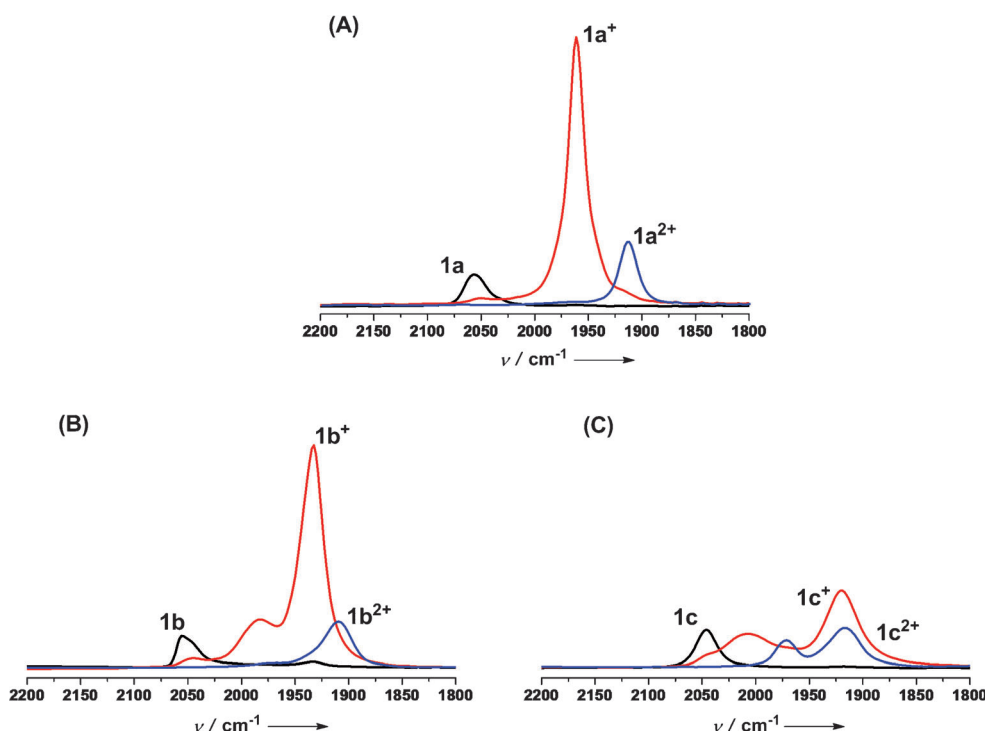


Figure 3. Changes in the IR spectra of complexes **1a**, **1b**, and **1c** in the presence of 0 (A, black line), 1.0 (B, red line), and 2.0 equiv of oxidant  $[\text{Cp}^*\text{Fe}]^+\text{PF}_6^-$  in  $\text{CH}_2\text{Cl}_2$  (C, blue line).

Table 4. UV/Vis/NIR electronic absorptions of compounds **1a–1c** in various oxidation states.

Complex	$\lambda_{\text{max}}$ [nm] ( $\epsilon_{\text{max}} \times 10^{-4}$ [ $\text{dm}^3 \text{mol}^{-1} \text{cm}^{-1}$ ])
<b>1a</b>	400 (2.51)
<b>[1a]<sup>+</sup></b>	600 (2.63), 1390 (2.11) <sup>[a]</sup>
<b>[1a]<sup>2+</sup></b>	754 (1.73)
<b>1b</b>	452 (1.97)
<b>[1b]<sup>+</sup></b>	754 (2.83), 1892 (3.19) <sup>[a]</sup>
<b>[1b]<sup>2+</sup></b>	908 (6.29)
<b>1c</b>	482 (3.98)
<b>[1c]<sup>+</sup></b>	780 (0.78), 2242 (0.80) <sup>[b]</sup>
<b>[1c]<sup>2+</sup></b>	414 (2.13), 1070 (2.39)

[a] Data for the main peak, which was not deconvoluted. [b] Data for a very broad peak within the NIR region.

500 nm) and gradually disappeared, possibly owing to a gradual collapse of the bridging ligand. These changes are also associated with the emergence of new bands in the visible-light region (500–1000 nm) and low-energy absorption bands between 1000 and 3000 nm (for detailed data, see Table 4). The absorptions in the visible-light region could be tentatively assigned to vibrationally structured aromatic radical bands, which implied a redox non-innocent character of the bridging ligand.<sup>[8b]</sup> For complexes **[1a]<sup>+</sup>**–**[1c]<sup>+</sup>**, broad bands were observed in the NIR region, which may be deconvoluted into the sum of three Gaussian-shaped sub-bands ( $\nu_1$ ,  $\nu_2$ , and  $\nu_3$ ), as shown in Figure 5 and the Supporting Information, Figures S3 and S4: Complex **[1a]<sup>+</sup>**:  $\nu_1 = 10758 \text{ cm}^{-1}$ ,  $\epsilon = 2738 \text{ dm}^3 \text{ mol}^{-1} \text{ cm}^{-1}$ ,  $\Delta\nu_{1/2} = 4370 \text{ cm}^{-1}$ ;  $\nu_2 = 9159 \text{ cm}^{-1}$ ,  $\epsilon = 13452 \text{ dm}^3 \text{ mol}^{-1} \text{ cm}^{-1}$ ,  $\Delta\nu_{1/2} = 2630 \text{ cm}^{-1}$ ;  $\nu_3 = 7046 \text{ cm}^{-1}$ ,  $\epsilon =$

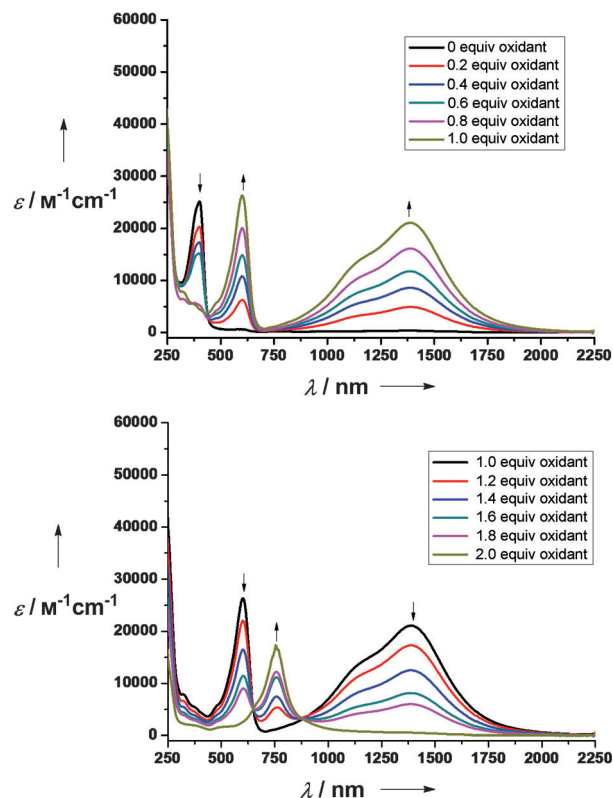


Figure 4. Changes in the UV/Vis/NIR electronic absorption spectra of complex **1a** in  $\text{CH}_2\text{Cl}_2$  after the gradual addition of ferrocenium hexafluorophosphate.

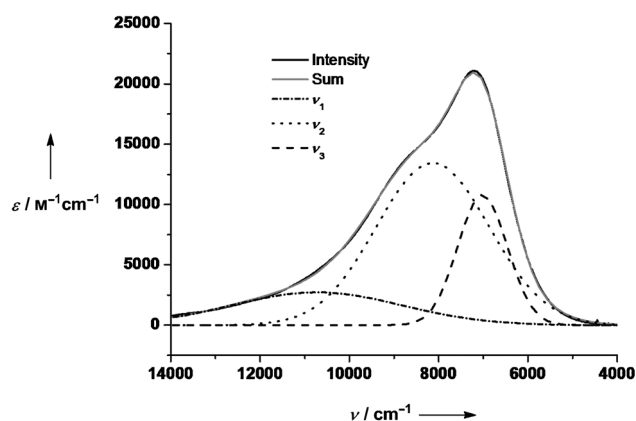


Figure 5. Deconvolution of the NIR spectra of monocation  $[1a]^+$ , which was generated by adding 1.0 equiv of  $[Cp^*_2Fe]^+PF_6^-$  in  $CH_2Cl_2$ .

$10792 \text{ dm}^3 \text{ mol}^{-1} \text{ cm}^{-1}$ ,  $\Delta\nu_{1/2}=1380 \text{ cm}^{-1}$ ; complex  $[1b]^+$ :  $\nu_1=7046 \text{ cm}^{-1}$ ,  $\epsilon=6127 \text{ dm}^3 \text{ mol}^{-1} \text{ cm}^{-1}$ ,  $\Delta\nu_{1/2}=3140 \text{ cm}^{-1}$ ;  $\nu_2=6369 \text{ cm}^{-1}$ ,  $\epsilon=11388 \text{ dm}^3 \text{ mol}^{-1} \text{ cm}^{-1}$ ,  $\Delta\nu_{1/2}=1880 \text{ cm}^{-1}$ ;  $\nu_3=5184 \text{ cm}^{-1}$ ,  $\epsilon=25982 \text{ dm}^3 \text{ mol}^{-1} \text{ cm}^{-1}$ ,  $\Delta\nu_{1/2}=1125 \text{ cm}^{-1}$ ; and complex  $[1c]^+$ :  $\nu_1=5944 \text{ cm}^{-1}$ ,  $\epsilon=4192 \text{ dm}^3 \text{ mol}^{-1} \text{ cm}^{-1}$ ,  $\Delta\nu_{1/2}=2230 \text{ cm}^{-1}$ ;  $\nu_2=3887 \text{ cm}^{-1}$ ,  $\epsilon=4926 \text{ dm}^3 \text{ mol}^{-1} \text{ cm}^{-1}$ ,  $\Delta\nu_{1/2}=1560 \text{ cm}^{-1}$ ;  $\nu_3=4836 \text{ cm}^{-1}$ ,  $\epsilon=5778 \text{ dm}^3 \text{ mol}^{-1} \text{ cm}^{-1}$ ,  $\Delta\nu_{1/2}=750 \text{ cm}^{-1}$ . The shape and intensity of the NIR band depend on many factors, such as redox-active end groups (spin-orbitals coupling),<sup>[8b,9b,38]</sup> the stability of the mixed-valence state ( $K_c$  value),<sup>[39]</sup> solvent effects,<sup>[40]</sup> and other factors;<sup>[41]</sup> on the other hand, the proportion of participation of the ligand orbitals and metal end groups in the frontier molecular orbitals (FMOs) also play an important role.<sup>[1c]</sup> For example, complex  $[[Fe(dppe)Cp^*_2](\mu-C\equiv C C_6H_4C\equiv C)]^{[18b]}$  has a “metal-dominated oxidation” character, whereas  $[[Fe(dppe)Cp^*_2](\mu-C\equiv C C_{14}H_8C\equiv C)]^{[18c]}$  has a more bridging character in the SOMO. Therefore, the shape and deconvolution analysis of NIR transitions can be used to preliminarily discuss the redox processes of these complexes. According to the pictures from deconvolution in complexes  $[1a]^+$  and  $[1b]^+$ , the  $\nu_3$  LMCT absorption band suggests that the ligand orbitals are involved in the oxidation process. On elongation of the thiophene bridging, the intensity of the  $\nu_3$  band clearly increases (from  $10792 \text{ dm}^3 \text{ mol}^{-1} \text{ cm}^{-1}$  in complex  $[1a]^+$  to  $25982 \text{ dm}^3 \text{ mol}^{-1} \text{ cm}^{-1}$  in complex  $[1b]^+$ ) and the involvement of ligand orbitals in the oxidation process becomes obvious. If the amount of ferrocenium hexafluorophosphate is gradually increased to 2.0 equivalents, the intensities of the transitions in the visible and NIR regions gradually decrease until they completely vanish, whilst a new MLCT transition appears. Complex  $[1c]^+$  produced weak NIR absorption bands, owing to the large separation between the bimetal ruthenium centers, which were clearly different to those of complexes  $[1a]^+$  and  $[1b]^+$ . Furthermore, complex  $[1c]^{2+}$  also displayed a strong MLCT band. These results suggest a strong participation of the bridging ligand in the oxidation processes. This result is further supported by using DFT calculations, as described below.

## DFT and TDDFT Calculations

To further understand the electronic properties of structures  $[1a]^{n+}$ ,  $[1b]^{n+}$ , and  $[1c]^{n+}$ , model complexes  $[1a-H]^{n+}$ ,  $[1b-H]^{n+}$ , and  $[1c-H]^{n+}$  ( $n=0, 1, 2$ ) were selected and density functional theory (DFT) calculations were performed at the B3LYP/3-21G\* level of theory, as described in the literature.<sup>[8b,i,28]</sup> The extension “-H” indicates that the  $\eta-C_5Me_5$  and dppe ligands are replaced by  $\eta-C_5H_5$  and two  $PH_3$  ligands. Selected frontier orbitals of structures  $[1a-H]$ ,  $[1b-H]$ , and  $[1c-H]$  are shown in Figure 6 and the Supporting Information, Figure S5. The orbital energies and the contributions of structures  $[1a]^{n+}$ – $[1c]^{n+}$  ( $n=0, 1, 2$ ), as given by Mulliken analysis, are shown in the Supporting Information, Tables S4–S11. In their neutral state, in which the HOMO is delocalized over the metal and the bridging ligands, these three model complexes show large contributions from the ethynyl oligothiophene moieties ( $[1a-H]$ : 78%;  $[1b-H]$ : 82%;  $[1c-H]$ : 86%). As a result of the large contribution of the bridging ligand to the HOMOs, subsequent oxidation of these complexes indicates that the dominant contributions may come from the unsaturated ligand orbitals. In the monocations of these complexes, according to Mulliken population analysis, the  $\beta$ -LUSOs have large contributions from the bridging ligand ( $[1a-H]^+$ : 72%;  $[1b-H]^+$ : 78%;  $[1c-H]^+$ : 82%), as shown in the Supporting Information, Tables S5, S8, and S11, respectively. On increasing the length of the thiophene rings and the distance between the two ruthenium centers, the contribution of the bridging ligand becomes more clear. We reason that this non-innocent behavior is highly dependent on the electronic character of the thiophene bridge. Furthermore, these results also indicate that the mixed-valence characteristics, which arise from the variation from delocalization to the localization of complexes  $[1a]^+$ – $[1c]^+$ , is consistent with the electrochemistry data and IR spectra (see above). This result can also be clearly visualized by the spin-density distribution (Figure 7),

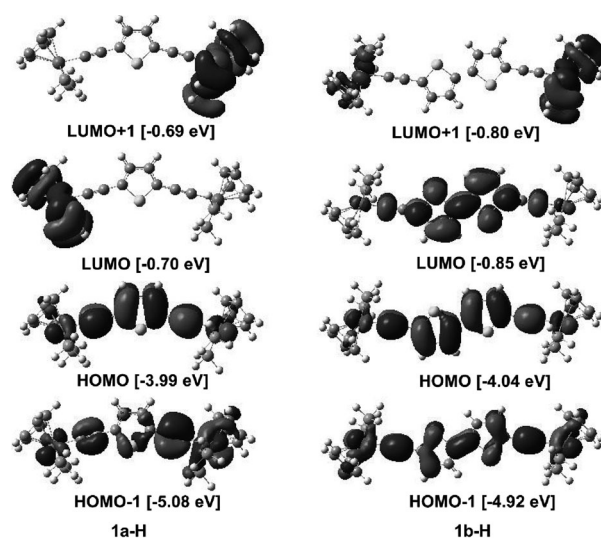


Figure 6. Selected frontier molecular orbitals of complexes  $[1a-H]$  and  $[1b-H]$ , plotted with contour values  $\pm 0.04$  ( $e \text{ bohr}^{-3}$ )<sup>1/2</sup>.

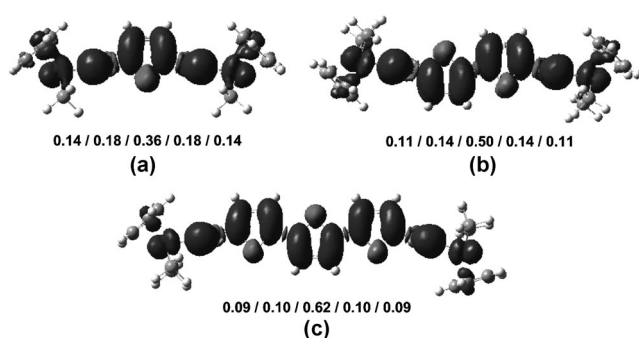


Figure 7. Spin-density distributions in a)  $[1\mathbf{a-H}]^+$ , b)  $[1\mathbf{b-H}]^+$ , and c)  $[1\mathbf{c-H}]^+$  with the corresponding compositions (Ru/C≡C/oligothiophene/C≡C/Ru). Contour values:  $\pm 0.04$  ( $e$  bohr $^{-3}$ ) $^{1/2}$ .

in which the metallic contribution decreased from 28% in structure  $[1\mathbf{a-H}]^+$  to 18% in structure  $[1\mathbf{c-H}]^+$ .

TDDFT calculations were performed on mono-oxidized species  $[1\mathbf{a-H}]^+$ ,  $[1\mathbf{b-H}]^+$ , and  $[1\mathbf{c-H}]^+$  to aid the assignment of their near-IR spectra. According to TDDFT predictions (Table 5), these absorptions are in agreement with previous assignments for similar monocations of bimetallic ruthenium–acetylide complexes.<sup>[8b,17]</sup> Selected frontier orbitals that are involved in the transitions for oxidized complexes  $[1\mathbf{a-H}]^+$ ,  $[1\mathbf{b-H}]^+$ , and  $[1\mathbf{c-H}]^+$  are shown in Figure 8. The major contributions to the absorptions at 853 nm ( $11719\text{ cm}^{-1}$ ) for structure  $[1\mathbf{a-H}]^+$ , 1080 nm ( $9251\text{ cm}^{-1}$ ) for structure  $[1\mathbf{b-H}]^+$ , and 1320 nm ( $7574\text{ cm}^{-1}$ ) for structure  $[1\mathbf{c-H}]^+$  come from the  $\beta$ -HOSO  $\rightarrow$   $\beta$ -LUSO and  $\alpha$ -HOSO  $\rightarrow$   $\alpha$ -LUSO transitions (Figure 8). These transitions have the same  $\text{IL-}\pi$ - $\pi^*$  character, mixed with LMCT or MLCT, and can be assigned to the observed NIR transitions, namely  $\nu_2$  and  $\nu_3$ , as identified by Gaussian deconvolution. TDDFT calculations revealed that the most-intense transitions appeared at 495, 590, and 668 nm for structures

Table 5. Major electronic excitations for cations  $[1\mathbf{a-H}]^+$ ,  $[1\mathbf{b-H}]^+$ , and  $[1\mathbf{c-H}]^+$ , as determined by using TDDFT methods (B3LYP/3-21G\* $^{[a]}$ ).

Compound	$\lambda$ [nm]	Oscillator strength ( $f$ )	Major contributions	Assignment
$[1\mathbf{a-H}]^+$	853.3	0.4603	$\alpha$ -HOSO $\rightarrow$ $\alpha$ -LUSO, $\beta$ -HOSO $\rightarrow$ $\beta$ -LUSO	LMCT IL- $\pi$ - $\pi^*$
	495.3	0.5106	$\alpha$ -HOSO $\rightarrow$ $\alpha$ -LUSO, $\beta$ -HOSO-6 $\rightarrow$ $\beta$ -LUSO,	MLCT ILCT/LMCT
	469	0.3191	$\beta$ -HOSO $\rightarrow$ $\beta$ -LUSO, $\alpha$ -HOSO $\rightarrow$ $\alpha$ -LUSO,	LMCT MLCT
			$\beta$ -HOSO-6 $\rightarrow$ $\beta$ -LUSO	ILCT/LMCT
$[1\mathbf{b-H}]^+$	1080.9	0.5064	$\alpha$ -HOSO $\rightarrow$ $\alpha$ -LUSO, $\beta$ -HOSO $\rightarrow$ $\beta$ -LUSO	LMCT IL- $\pi$ - $\pi^*$
	590.3	1.3403	$\alpha$ -HOSO $\rightarrow$ $\alpha$ -LUSO, $\beta$ -HOSO-3 $\rightarrow$ $\beta$ -LUSO+1	LMCT MLCT
	446.3	0.1364	$\alpha$ -HOSO-6 $\rightarrow$ $\alpha$ -LUSO, $\alpha$ -HOSO $\rightarrow$ $\alpha$ -LUSO,	MLCT LMCT
			$\beta$ -HOSO-6 $\rightarrow$ $\beta$ -LUSO	MLCT
$[1\mathbf{c-H}]^+$	1320.3	0.6224	$\beta$ -HOSO $\rightarrow$ $\beta$ -LUSO, $\alpha$ -HOSO $\rightarrow$ $\alpha$ -LUSO,	IL- $\pi$ - $\pi^*$ MLCT
	668.6	1.6673	$\beta$ -HOSO-6 $\rightarrow$ $\beta$ -LUSO, $\beta$ -HOSO $\rightarrow$ $\beta$ -LUSO	MLCT ILCT
	522.4	0.0927	$\beta$ -HOSO-6 $\rightarrow$ $\beta$ -LUSO	ILCT

[a] MLCT = metal to ligand charge transfer, ILCT = intraligand charge transfer, LMCT = ligand to metal charge transfer, IL = intraligand.

$[1\mathbf{a-H}]^+$ ,  $[1\mathbf{b-H}]^+$ , and  $[1\mathbf{c-H}]^+$ , with oscillator strengths of 0.51, 1.34, and 1.66, respectively. These transitions have dominant contributions from vibrationally structured aromatic radical bands, in good agreement with previous bimetallic systems.<sup>[8b]</sup> These bands consist of  $\beta$ -HOSO-6  $\rightarrow$   $\beta$ -LUSO and  $\alpha$ -HOSO  $\rightarrow$   $\alpha$ -LUSO excitations for structures  $[1\mathbf{a-H}]^+$  and  $[1\mathbf{c-H}]^+$  and  $\beta$ -HOSO-3  $\rightarrow$   $\beta$ -LUSO+1 and  $\alpha$ -HOSO  $\rightarrow$   $\alpha$ -LUSO excitations for structure  $[1\mathbf{b-H}]^+$ .

## EPR Spectroscopy

EPR spectroscopy is a highly sensitive technique that has been used to evaluate the contributions of metal centers and bridging ligands to redox processes. Detailed information can be obtained from  $g$  values, which can provide significant information concerning molecular structure and environmental variables. Accordingly, we performed EPR experiments for each of the monocations in  $\text{CH}_2\text{Cl}_2$  at 298 K and 150 K. The EPR spectra of structures  $[1\mathbf{a}]^+$ ,  $[1\mathbf{b}]^+$ , and  $[1\mathbf{c}]^+$  were collected after the addition of 1.0 equivalents of ferrocenium hexafluorophosphate in  $\text{CH}_2\text{Cl}_2$  at 298 and 150 K. The results are shown in Figure 9 and the Supporting Information, Figures S6 and S7; the details are summarized in Table 6. At 298 K, these cations show a peaked isotropic signal, for which all of the  $g$  values are about 2.04 and show the characteristics of a free electron. However, when the temperature was cooled to 150 K, broad isotropic signals were found for all of the monocations. The  $g$  tensors exhibited modest splitting that was comparable with that at 298 K, which could be attributed to slow relaxation of the free electron at low temperatures. The free electron that is localized on an organometallic ruthenium(III) center usually exhibits a  $\Delta g$  value of between 0.3 and 0.6.<sup>[29]</sup> We calculated the total  $g$  anisotropy ( $\Delta g$ ) values of structures  $[1\mathbf{a}]^+$ ,  $[1\mathbf{b}]^+$ , and  $[1\mathbf{c}]^+$  to be 0.042, 0.027, and 0.052, respectively. Structures  $[1\mathbf{a}]^+$  and  $[1\mathbf{c}]^+$  have larger  $\Delta g$  values than structure  $[1\mathbf{b}]^+$ , as a result of variation in electron delocalization. The low  $g_{\text{iso}}$  and  $\Delta g$  values also indicate a significant participation of ligand oxidation,<sup>[24,35]</sup> which further supports the previous analysis of the experimental data and the DFT calculations.

## Conclusions

To summarize, we have synthesized a series of binuclear ruthenium–alkynyl complexes that were bridged by thiophene groups (thiophene, bithiophene, and terthiophene). All of these complexes were structurally characterized by using NMR spectroscopy, X-ray diffraction, and elemental analysis. Their electronic properties have been examined by using electrochemistry, IR and UV/Vis/NIR spectroscopy, and EPR spectroscopy. Electrochemical studies indicate that the stability of these mono-oxidized states decreases as the bridging ligand lengths from thiophene to terthiophene. The character-

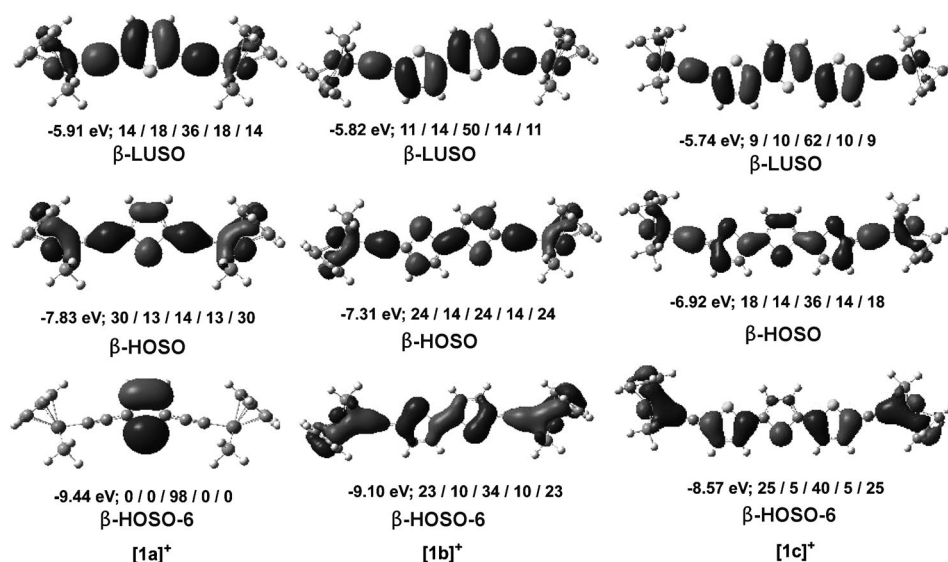


Figure 8. Selected frontier orbitals that are involved in the transitions for mono-oxidized complexes  $[1a-H]^+$ ,  $[1b-H]^+$ , and  $[1c-H]^+$ . Contour values:  $\pm 0.04$  ( $e \text{ bohr}^{-3}$ )<sup>1/2</sup>. Orbital energies and the corresponding compositions (Cp(PH<sub>3</sub>)<sub>2</sub>Ru/C<sub>2</sub>/oligothiophene/C<sub>2</sub>/Ru(PH<sub>3</sub>)<sub>2</sub>Cp) are also provided.

istic absorptions of the C≡C bonds in these complexes within the IR range upon step-wise chemical oxidation indicate that the bridging ligands have an important effect on the redox processes of the complexes. The UV/Vis/NIR spectra of monocations  $[1a-1c]^+$  exhibit clear MLCT and ILCT characteristics and have been well-assigned with the assistance of TDDFT calculations. EPR spectroscopy and

DFT calculations (spin-density-distribution analysis) suggest that the mono-oxidized radical species of these complexes have significant characteristics of the bridging ligands and all of these bimetallic ruthenium complexes display a redox non-innocent ligand behavior. This study of the electronic properties of these complexes provides significant guidelines for the design and synthesis of new mixed-valence systems with potential applications in molecular electronics. Our future work will continue to focus on the preparation of new bridging ligands and on the construction of other mixed-valence complexes.

## Experimental Section

### General Materials

All manipulations were carried out at RT under a nitrogen atmosphere by using standard Schlenk techniques, unless otherwise stated. Solvents were pre-dried, distilled, and degassed prior to use, except for those that were for spectroscopic measurements, which were of spectroscopic grade. The reagents 2-bromothiophene and 2,5-dibromothiophene (**2a**) were commercially available. The starting materials [Cp\*(dppe)RuCl],<sup>[30]</sup> 5,5'-dibromo-2,2'-bithiophene (**2b**),<sup>[31]</sup> and 5,5'-dibromo-2,2':5',2''-terthiophene (**2c**)<sup>[32]</sup> were prepared according to literature procedures.

### Synthesis of the Bis(trimethylsilyl)ethynyloligothiophenes

**2,5-Bis(trimethylsilylethynyl)thiophene (3a)**: To a stirring solution of 2,5-dibromothiophene (**2a**, 1 g, 4.1 mmol), CuI (38 mg, 0.20 mmol), and [Pd(PPh<sub>3</sub>)<sub>4</sub>] (477 mg, 0.41 mmol) in triethylamine (40 mL) and THF (60 mL) under an argon atmosphere was added (trimethylsilyl)acetylene (1.18 g, 12 mmol) and the mixture was heated at reflux (60°C) for 24 h. The cold solution was filtered through a pad of celite. The filtrate was evaporated under reduced pressure and purified by column chromatography on silica gel (petroleum ether) to give a light-yellow solid (910 mg, 80% yield). <sup>1</sup>H NMR (400 MHz, CDCl<sub>3</sub>):  $\delta$  = 0.19 (s, 18H; SiCH<sub>3</sub>), 6.95 (d,  $J$  = 3.6 Hz, 1H; thiophene-H), 7.07 ppm (d,  $J$  = 3.6 Hz, 1H; thiophene-H).

**5,5'-Bis(trimethylsilylethynyl)-2,2'-bithiophene (3b)**: The procedure for the synthesis of compound **3b** was similar to that for compound **3a**, with

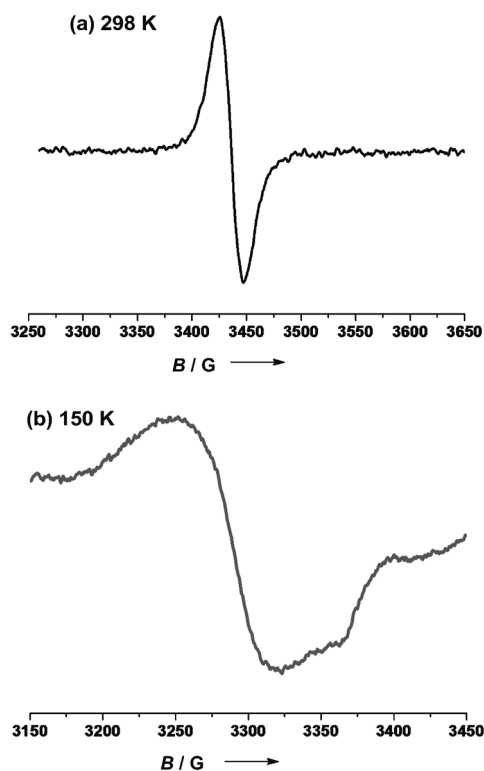


Figure 9. EPR spectra of monocation  $[1a]^+$ , which was generated by adding 1.0 equiv of [Cp\*<sub>2</sub>Fe]<sup>+</sup>PF<sub>6</sub><sup>-</sup> in CH<sub>2</sub>Cl<sub>2</sub> at a) 298 K and b) 150 K.

Table 6. EPR spectroscopic data of monocations  $[1a]^+$ ,  $[1b]^+$ , and  $[1c]^+$ .

Cation	$g_{\text{iso}}$ (298 K) <sup>[a]</sup>	$g$ (150 K) <sup>[b]</sup>	$\Delta g^{[c]}$
$[1a]^+$	2.046	$g_1 = g_2 = 2.053,$ $g_3 = 2.011,$ $g_{\text{av}} = 2.039$	0.042
$[1b]^+$	2.042	$g_1 = g_2 = 2.036,$ $g_3 = 2.009,$ $g_{\text{av}} = 2.027$	0.027
$[1c]^+$	2.049	$g_1 = g_2 = 2.052,$ $g_3 = 2.000,$ $g_{\text{av}} = 2.034$	0.052

[a]  $g_{\text{iso}}$  = isotropic  $g$  value. [b]  $g_{\text{av}}$  = average  $g$  value, calculated according to  $[(g_1^2 + g_2^2 + g_3^2)/3]^{1/2}$ . [c] Total  $g$  anisotropy,  $\Delta g = g_1 - g_3$ .

compound **2b** (2.0 g, 6.94 mmol), CuI (64 mg, 0.35 mmol), [Pd(PPh<sub>3</sub>)<sub>4</sub>] (803 mg, 0.69 mmol), triethylamine (60 mL), THF (100 mL), and (trimethylsilyl)acetylene (2.04 g, 20.8 mmol). Yield: 1.62 g (65%); light-yellow solid; <sup>1</sup>H NMR (400 MHz, CDCl<sub>3</sub>): δ = 0.24 (s, 18H; SiCH<sub>3</sub>), 6.99 (d, *J* = 3.6 Hz, 2H; thiophene-H), 7.12 ppm (d, *J* = 3.6 Hz, 2H; thiophene-H).

**5,5'-Bis(trimethylsilylethynyl)-2,2':5',2'-terthiophene(3c)**: The procedure for the synthesis of compound **3c** was similar to that for compound **3a**, with compound **2c** (0.7 g, 1.72 mmol), CuI (33 mg, 0.17 mmol), [Pd(PPh<sub>3</sub>)<sub>4</sub>] (199 mg, 0.17 mmol), (iPr)<sub>2</sub>NH (30 mL), THF (30 mL), and (trimethylsilyl)acetylene (675 mg, 6.89 mmol). Yield: 300 mg (59%); light-yellow solid; <sup>1</sup>H NMR (400 MHz, CDCl<sub>3</sub>): δ = 0.26 (s, 18H; SiCH<sub>3</sub>), 7.01 (d, *J* = 4.0 Hz, 2H; thiophene-H), 7.07 (s, 2H; thiophene-H), 7.13 ppm (d, *J* = 4.0 Hz, 2H; thiophene-H).

#### Synthesis of the Binuclear Ruthenium Complexes

**Compound 1a**: A solution of [Cp\*(dppe)RuCl] (387 mg, 0.58 mmol), 2,5-bis(trimethylsilylethynyl)thiophene (**3a**, 80 mg, 0.29 mmol), and KF (202 mg, 3.47 mmol) in MeOH (20 mL) and THF (5 mL) was heated at reflux under a nitrogen atmosphere for 24 h. The crude product was collected by filtration and washed with MeOH and *n*-hexane. The solid was dissolved in CH<sub>2</sub>Cl<sub>2</sub> and precipitated by slow diffusion with *n*-hexane. The solid was filtered and dried to give compound **1a** as a red-brown powder (250 mg, 60%). <sup>1</sup>H NMR (400 MHz, CDCl<sub>3</sub>): δ = 1.54 (s, 30H; 2 × C<sub>5</sub>(CH<sub>3</sub>)<sub>3</sub>), 2.04 (br s, 4H; CH<sub>2</sub>/dppe), 2.67 (br s, 4H; CH<sub>2</sub>/dppe), 7.20–7.37 (m, 32H+2H; H<sub>Ari(dppe)</sub>+H<sub>thiophene</sub>), 7.77 ppm (br s, 8H; H<sub>Ari(dppe)</sub>); <sup>13</sup>C NMR (100 MHz, CDCl<sub>3</sub>): δ = 9.94 (CH<sub>3</sub>), 29.42 (t, *J* = 22.80 Hz; CH<sub>2</sub>/dppe), 92.62 (CH/C<sub>3</sub>Me<sub>3</sub>), 101.66 (thiophene-C), 123.65 (Ru-C), 127.28, 128.75, 133.24, 133.71, 136.77, 137.16, 138.84 ppm; <sup>31</sup>P NMR (160 MHz, CDCl<sub>3</sub>): δ = 78.01 ppm (dppe); IR (KBr):  $\tilde{\nu}$  = 2064 cm<sup>-1</sup> (w, C≡C); elemental analysis calcd (%) for C<sub>80</sub>H<sub>80</sub>P<sub>4</sub>Ru<sub>2</sub>S<sub>2</sub>: C 68.65, H 5.76; found: C 68.63, H 5.77.

**Compound 1b**: The procedure for the synthesis of compound **1b** was similar to that for compound **1a**, with [Cp\*(dppe)RuCl] (275 mg, 0.41 mmol), 5,5'-bis(trimethylsilylethynyl)-2,2'-bithiophene (**3b**, 70 mg, 0.20 mmol), KF (136 mg, 2.35 mmol), MeOH (20 mL), and THF (5 mL). Yield: 130 mg (44%); light-yellow solid; <sup>1</sup>H NMR (400 MHz, CDCl<sub>3</sub>): δ = 1.59 (s, 30H; 2 × C<sub>5</sub>(CH<sub>3</sub>)<sub>3</sub>), 2.05 (br s, 4H; CH<sub>2</sub>/dppe), 2.65 (br s, 4H; CH<sub>2</sub>/dppe), 7.22–7.38 (m, 32H+4H; H<sub>Ari(dppe)</sub>+H<sub>thiophene</sub>), 7.74 ppm (br s, 8H; H<sub>Ari(dppe)</sub>); <sup>31</sup>P NMR (160 MHz, CDCl<sub>3</sub>): δ = 79.90 ppm (dppe); IR (KBr):  $\tilde{\nu}$  = 2056 cm<sup>-1</sup> (w, C≡C); elemental analysis calcd (%) for C<sub>84</sub>H<sub>82</sub>P<sub>4</sub>Ru<sub>2</sub>S<sub>2</sub>: C 68.09, H 5.58; found: C 68.21, H 5.34. Note: This compound has poor solubility in many deuterated solvents, including CDCl<sub>3</sub>, in which the <sup>13</sup>C NMR spectrum could not be recorded.

**Compound 1c**: The procedure for the synthesis of compound **1c** was similar to that for compound **1a**, with [Cp\*(dppe)RuCl] (319 mg, 0.48 mmol), 5,5'-bis(trimethylsilylethynyl)-2,2':5',2'-terthiophene (**3c**, 100 mg, 0.23 mmol), KF (158 mg, 2.72 mmol), MeOH (20 mL), and THF (5 mL). Crystals suitable for X-ray crystallography were grown from the slow diffusion of *n*-hexane into a solution of compound **1c** in CH<sub>2</sub>Cl<sub>2</sub>. Yield: 190 mg (54%); purple powder; <sup>1</sup>H NMR (400 MHz, CDCl<sub>3</sub>): δ = 1.55 (s, 30H; 2 × C<sub>5</sub>(CH<sub>3</sub>)<sub>3</sub>), 2.05 (br s, 4H; CH<sub>2</sub>/dppe), 2.67 (br s, 4H; CH<sub>2</sub>/dppe), 6.18 (s, 2H; thiophene), 6.77 (d, *J*(H,H) = 3.6 Hz, 2H; thiophene), 6.81 (s, 2H; thiophene), 7.20–7.37 (m, 32H; H<sub>Ari(dppe)</sub>), 7.74 ppm (br s, 8H; H<sub>Ari(dppe)</sub>); <sup>13</sup>C NMR (100 MHz, CDCl<sub>3</sub>): δ = 10.11 (CH<sub>3</sub>), 29.59 (t, *J* = 22.80 Hz, CH<sub>2</sub>/dppe), 92.86 (CH/C<sub>3</sub>Me<sub>3</sub>), 102.32 (thiophene-C), 122.41, 122.67, 122.87, 125.10 (Ru-C), 127.58, 128.97, 129.17, 130.69, 131.90, 133.24, 133.39, 133.73, 135.79, 136.00, 136.33, 136.53, 136.80, 137.01, 138.49, 138.82, 141.29 ppm; <sup>31</sup>P NMR (160 MHz, CDCl<sub>3</sub>): δ = 79.93 ppm (dppe); IR (KBr):  $\tilde{\nu}$  = 2046 cm<sup>-1</sup> (w, C≡C); elemental analysis calcd (%) for C<sub>88</sub>H<sub>84</sub>P<sub>4</sub>Ru<sub>2</sub>S<sub>3</sub>: C 67.59, H 5.41; found: C 67.71, H 5.26.

#### Crystallographic Details

Single crystals of complex **1c** suitable for X-ray analysis were obtained by the slow diffusion of *n*-hexane into a solution in CH<sub>2</sub>Cl<sub>2</sub>. Crystals with approximate dimensions of 0.16 × 0.12 × 0.10 mm<sup>3</sup> were mounted onto glass fibers for the diffraction experiments. Intensity data were collected on a Nonius Kappa CCD diffractometer with MoK<sub>α</sub> radiation (0.71073 Å) at low temperatures (100 K). The structure was solved by using a combi-

nation of direct methods (SHELXS-97)<sup>[33]</sup> and Fourier difference techniques and were refined by full-matrix least-squares (SHELXL-97).<sup>[34]</sup> All non-H atoms were refined anisotropically. The hydrogen atoms were placed at ideal positions and refined as riding atoms. The solvent molecules in compound **1c** could not be refined because of their highly disordered structure. Therefore, the SQUEEZE function of the PLATON program was used to eliminate the contribution of the electron density in the solvent region from the intensity data.<sup>[37]</sup> The contribution of these species was removed and final refinement was performed. Partial solvent molecules were omitted. Further crystal data and details of the data collection are summarized in the Supporting Information, Table S1. Selected bond lengths and angles are given in Table 1. CCDC 941574 (**1c**) contains the supplementary crystallographic data for this paper. These data can be obtained free of charge from The Cambridge Crystallographic Data Centre via www.ccdc.cam.ac.uk/data\_request/cif.

#### Physical Measurements

<sup>1</sup>H, <sup>13</sup>C, and <sup>31</sup>P NMR spectra were collected on a Varian Mercury Plus 400 spectrometer (400 MHz). <sup>1</sup>H and <sup>13</sup>C NMR chemical shifts are reported relative to TMS and <sup>31</sup>P NMR chemical shifts are reported relative to 85% H<sub>3</sub>PO<sub>4</sub>. Elemental analysis was performed on a Vario EIII Chno instrument. UV/Vis/NIR spectra were recorded on a Shimadzu UV-3600 UV/Vis/NIR spectrophotometer by using liquid sample cells (path length: 200 μm). IR spectra were recorded on a Nicolet Avatar spectrometer from Nujol mulls that were suspended between KBr discs and liquid sample cells (path length: 200 μm). The electrochemical measurements were performed on a CHI 660C potentiostat (CHI USA). A three-electrode one-compartment cell was used to contain the solution of complexes and supporting electrolyte in dry CH<sub>2</sub>Cl<sub>2</sub>. De-aeration of the solution was achieved by bubbling argon gas through the solution for about 10 min before the measurements. The concentrations of the ligand and the electrolyte (nBu<sub>4</sub>NPF<sub>6</sub>) were typically 0.001 and 0.1 mol dm<sup>-3</sup>, respectively. A platinum disk working electrode (diameter: 500 μm), a platinum wire counter electrode, and a Ag/Ag<sup>+</sup> reference electrode were used. The Ag/Ag<sup>+</sup> reference electrode contained a 0.01 M AgNO<sub>3</sub> solution in CH<sub>3</sub>CN. Chemical oxidation experiments of the charge-neutral molecules were carried out: Monocationic and dicationic forms were affected by ferrocenium hexafluorophosphate, in accord with the results of the electrochemical oxidation. EPR spectroscopy was performed on a Bruker BioSpin GmbH, by using a microwave frequency of about 9.84 GHz, a modulation frequency of 100 kHz, a modulation amplitude of 1 G, and about a microwave power 20 mW.

#### Computational Details

DFT calculations were performed by using the Gaussian 03 and 09 programs at the B3LYP/3-21G\* level of theory. Geometry optimizations were performed without any symmetry constraints and frequency calculations on the resulting optimized geometries showed no imaginary frequencies. Electronic transitions were calculated by using the time-dependent DFT (TDDFT) method. The MO contributions were generated by using the Multiwfn2.6.1\_bin\_Win package and plotted by using GaussView 5.0.

## Acknowledgements

The authors acknowledge financial support from the National Natural Science Foundation of China (20931006, 21072070, 21072071, and 21272088), the Program for Changjiang Scholars and Innovative Research Team in University (IRT0953), and the Program for Academic Leader in Wuhan Municipality (201271130441).

- [1] a) J. Hankache, O. S. Wenger, *Chem. Rev.* **2011**, *111*, 5138–5178; b) A. Cecon, S. Santi, L. Oriani, A. Bisello, *Coord. Chem. Rev.* **2004**, *248*, 683–724; c) P. Aguirre-Etcheverry, D. O'Hare, *Chem. Rev.* **2010**, *110*, 4839–4864.

- [2] a) T.-Y. Dong, K. Chen, M.-C. Lin, L. Lee, *Organometallics* **2005**, *24*, 4198–4206; b) Y. Lee, S. R. Jang, R. Vittal, K. J. Kim, *New J. Chem.* **2007**, *31*, 2120–2126; c) K. L. McCall, G. R. Jennings, H. Wang, A. Morandeira, L. M. Peter, J. R. Durrant, L. J. Yellowlees, N. Robertson, *Eur. J. Inorg. Chem.* **2011**, 589–596; d) Y. Ou, G. Chen, J. Yin, G.-A. Yu, S. H. Liu, *J. Coord. Chem.* **2011**, *64*, 3062–3067.
- [3] A. Yoshimura, M. J. Uddin, N. Amashaki, T. Ohno, *J. Phys. Chem. A* **2001**, *105*, 10846–10853.
- [4] L. Luo, A. Benameur, P. Brignou, S. H. Choi, S. Rigaut, C. D. Frisbie, *J. Phys. Chem. C* **2011**, *115*, 19955–19961.
- [5] C. Creutz, H. Taube, *J. Am. Chem. Soc.* **1969**, *91*, 3988–3989.
- [6] For oligoethynyl-bridged biruthenium complexes, see: a) G.-L. Xu, G. Zou, Y.-H. Ni, M. C. DeRosa, R. J. Crutchley, T. Ren, *J. Am. Chem. Soc.* **2003**, *125*, 10057–10065; b) G. L. Xu, R. J. Crutchley, M. C. DeRosa, Q. J. Pan, H. X. Zhang, X. Wang, T. Ren, *J. Am. Chem. Soc.* **2005**, *127*, 13354–13363; c) J.-W. Ying, I. P. C. Liu, B. Xi, Y. Song, C. Campana, J. L. Zuo, T. Ren, *Angew. Chem.* **2010**, *122*, 966–969; *Angew. Chem. Int. Ed.* **2010**, *49*, 954–957; d) B. Xi, I. P. C. Liu, G. L. Xu, M. M. R. Choudhuri, M. C. DeRosa, R. J. Crutchley, T. Ren, *J. Am. Chem. Soc.* **2011**, *133*, 15094–15104; e) Q. Zheng, J. A. Gladysz, *J. Am. Chem. Soc.* **2005**, *127*, 10508–10509; f) J. Stahl, W. Mohr, L. de Quadras, T. B. Peters, J. C. Bohling, J. M. Martín-Alvarez, G. R. Owen, F. Hampel, J. A. Gladysz, *J. Am. Chem. Soc.* **2007**, *129*, 8282–8295; g) H. Qi, A. Gupta, B. C. Noll, G. L. Snider, Y. Lu, C. Lent, T. P. Fehlner, *J. Am. Chem. Soc.* **2005**, *127*, 15218–15227; h) M. I. Bruce, P. J. Low, K. Costuas, J.-F. Halet, S. P. Best, G. A. Heath, *J. Am. Chem. Soc.* **2000**, *122*, 1949–1962.
- [7] For oligovinyl-bridged biruthenium complexes, see: a) S. H. Liu, Y. Chen, K. L. Wan, T. B. Wen, Z. Zhou, M. F. Lo, I. D. Williams, G. Jia, *Organometallics* **2002**, *21*, 4984–4992; b) S. H. Liu, H. Xia, T. B. Wen, Z. Y. Zhou, G. Jia, *Organometallics* **2003**, *22*, 737–743; c) L.-B. Gao, S.-H. Liu, L.-Y. Zhang, L.-X. Shi, Z.-N. Chen, *Organometallics* **2006**, *25*, 506–512; d) S. H. Liu, Q. Y. Hu, P. Xue, T. B. Wen, I. D. Williams, G. Jia, *Organometallics* **2005**, *24*, 769–772; e) P. Yuan, X. H. Wu, G. Yu, D. Du, S. H. Liu, *J. Organomet. Chem.* **2007**, *692*, 3588–3592.
- [8] For aryl-bridged biruthenium complexes, see: a) M. A. Fox, B. L. Guennic, R. L. Roberts, T. E. Baines, D. S. Yufit, D. Albesa-Jové, J. F. Halet, F. Hartl, J. A. K. Howard, P. J. Low, *J. Am. Chem. Soc.* **2008**, *130*, 3566–3578; b) M. A. Fox, B. L. Guennic, R. L. Roberts, D. A. Brue, D. S. Yufit, J. A. K. Howard, G. Manca, J.-F. Halet, F. Hartl, P. J. Low, *J. Am. Chem. Soc.* **2011**, *133*, 18433–18446; c) S. Ibn Ghazala, F. Paul, L. Toupet, T. Roisnel, P. Hapiot, C. Lapinte, *J. Am. Chem. Soc.* **2006**, *128*, 2463–2476; d) C.-J. Yao, Y. W. Zhong, J. Yao, *J. Am. Chem. Soc.* **2011**, *133*, 15697–15706; e) L. Wang, W.-W. Yang, R. H. Zheng, Q. Shi, Y. W. Zhong, J. Yao, *Inorg. Chem.* **2011**, *50*, 7074–7079; f) M. Linseis, S. Zális, M. Zabel, R. F. Winter, *J. Am. Chem. Soc.* **2012**, *134*, 16671–16692; g) E. Anger, M. Srebro, N. Vanthuyne, L. Toupet, S. Rigaut, C. Roussel, J. Autschbach, J. Crasous, R. Réau, *J. Am. Chem. Soc.* **2012**, *134*, 15628–15631; h) Y.-P. Ou, C. Jiang, D. Wu, J. Xia, J. Yin, S. Jin, G.-A. Yu, S. H. Liu, *Organometallics* **2011**, *30*, 5763–5770; i) J.-L. Xia, W. Y. Man, X. Zhu, C. Zhang, G. J. Jin, P. A. Schauer, M. A. Fox, J. Yin, G.-A. Yu, P. J. Low, S. H. Liu, *Organometallics* **2012**, *31*, 5321–5333.
- [9] a) C. Lapinte, *J. Organomet. Chem.* **2008**, *693*, 793–801; b) K. Costuas, O. Cador, F. Justaud, S. L. Stang, F. Paul, A. Monari, S. Evangelisti, L. Toupet, C. Lapinte, J.-F. Halet, *Inorg. Chem.* **2011**, *50*, 12601–12622; c) R. Z. Sui, W. W. Yang, C.-J. Yao, H.-Y. Xie, Y. W. Zhong, *Inorg. Chem.* **2012**, *51*, 1590–1598.
- [10] *Handbook of Oligo- and Polythiophenes* (Ed.: D. Fichou), Wiley-VCH, Weinheim, **1999**.
- [11] H. Qu, C. Chi, *Curr. Org. Chem.* **2010**, *14*, 2070–2108.
- [12] K. Niimi, S. Shinamura, I. Osaka, E. Miyazaki, K. Takimiya, *J. Am. Chem. Soc.* **2011**, *133*, 8732–8739.
- [13] R. Kumar, R. G. Pillai, N. Pekas, Y. Wu, R. L. McCreery, *J. Am. Chem. Soc.* **2012**, *134*, 14869–14876.
- [14] T. L. Stott, M. O. Wolf, *Coord. Chem. Rev.* **2003**, *246*, 89–101.
- [15] L. G. Reuter, A. G. Bonn, A. C. Stückl, B. He, B. B. Pati, S. S. Zade, O. S. Wenger, *J. Phys. Chem. A* **2012**, *116*, 7345–7352.
- [16] L.-B. Gao, J. Kan, Y. Fan, L.-Y. Zhang, S. H. Liu, Z.-N. Chen, *Inorg. Chem.* **2007**, *46*, 5651–5664.
- [17] X. Zhu, Y. Ou, J. Zhang, J.-L. Xia, J. Yin, G.-A. Yu, S. H. Liu, *Dalton Trans.* **2013**, *42*, 7177–7189.
- [18] a) P. Hamon, F. Justaud, O. Cador, P. Hapiot, S. Rigaut, L. Toupet, L. Ouahab, H. Stueger, J.-R. Hamon, C. Lapinte, *J. Am. Chem. Soc.* **2008**, *130*, 17372–17383; b) N. Le Narvor, C. Lapinte, *Organometallics* **1995**, *14*, 634–639; c) F. de Montigny, G. Argouarch, K. Costuas, J. F. Halet, T. Roisnel, L. Toupet, C. Lapinte, *Organometallics* **2005**, *24*, 4558–4572.
- [19] a) S. Frayse, C. Coudret, J.-P. Launay, *J. Am. Chem. Soc.* **2003**, *125*, 5880–5888; b) W. Kaim, G. K. Lahiri, *Angew. Chem.* **2007**, *119*, 1808–1828; *Angew. Chem. Int. Ed.* **2007**, *46*, 1778–1796.
- [20] F. Paul, C. Lapinte, *Coord. Chem. Rev.* **1998**, *178*, 431–509.
- [21] B. Kim, J. M. Beebe, C. Olivier, S. Rigaut, D. Touchard, J. G. Kushmerick, X. Y. Zhu, C. D. Frisbie, *J. Phys. Chem. C* **2007**, *111*, 7521–7526.
- [22] K. Kowalski, M. Linseis, R. F. Winter, M. Zabel, S. Zalis, H. Kelm, H. J. Kruger, B. Sarkar, W. Kaim, *Organometallics* **2009**, *28*, 4196–4209.
- [23] M. A. Fox, J. D. Farmer, R. L. Roberts, M. G. Humphrey, P. J. Low, *Organometallics* **2009**, *28*, 5266–5269.
- [24] J. Maurer, B. Sarkar, W. Kaim, R. F. Winter, S. Zális, *Chem. Eur. J.* **2007**, *13*, 10257–10272.
- [25] N. G. Connelly, W. E. Geiger, *Chem. Rev.* **1996**, *96*, 877–910.
- [26] M. Sato, H. Shintate, Y. Kawata, M. Sekino, M. Katada, S. Kawata, *Organometallics* **1994**, *13*, 1956–1962.
- [27] D. J. Armit, M. I. Bruce, M. Gaudio, N. N. Zaitseva, B. W. Skelton, A. H. White, B. L. Guennic, J.-F. Halet, M. A. Fox, R. L. Roberts, F. Hartl, P. J. Low, *Dalton Trans.* **2008**, 6763–6775.
- [28] a) C. Daul, C. Rauzy, S. Decurtins, P. Franz, A. Hauser, *Int. J. Quantum Chem.* **2005**, *101*, 753–760; b) S. Kababya, J. Nelson, C. Calle, F. Neese, D. Goldfarb, *J. Am. Chem. Soc.* **2006**, *128*, 2017–2029.
- [29] a) T. Sixt, J. Fiedler, W. Kaim, *Inorg. Chem. Commun.* **2000**, *3*, 80–82; b) R. F. Winter, F. M. Hornung, *Organometallics* **1999**, *18*, 4005–4014.
- [30] M. I. Bruce, B. G. Ellis, P. J. Low, B. W. Skelton, A. H. White, *Organometallics* **2003**, *22*, 3184–3198.
- [31] Y. A. Getmanenko, R. J. Twieg, *J. Org. Chem.* **2008**, *73*, 830–839.
- [32] E. Kozma, F. Munno, D. Kotowski, F. Bertini, S. Luzzati, M. Catellani, *Synth. Met.* **2010**, *160*, 996–1001.
- [33] G. M. Sheldrick, SHELXS-97, a Program for Crystal Structure Solution; University of Göttingen: Göttingen, Germany, **1997**.
- [34] G. M. Sheldrick, SHELXL-97, a Program for Crystal Structure Refinement; University of Göttingen, Göttingen, Germany, **1997**.
- [35] J. Maurer, B. Sarkar, B. Schwederski, W. Kaim, R. F. Winter, S. Zális, *Organometallics* **2006**, *25*, 3701–3712.
- [36] N. J. Brown, H. N. Lancashire, M. A. Fox, D. Collison, R. Edge, D. S. Yufit, J. A. K. Howard, M. W. Whiteley, P. J. Low, *Organometallics* **2011**, *30*, 884–894.
- [37] P. Van der Sluis, A. L. Spek, *Acta Crystallogr. Sect. A* **1990**, *46*, 194–201.
- [38] a) A. Hildebrandt, D. Schaarschmidt, R. Claus, H. Lang, *Inorg. Chem.* **2011**, *50*, 10623–10632; b) A. Donoli, A. Bisello, R. Cardena, C. Prinzivalli, S. Santi, *Organometallics* **2013**, *32*, 1029–1036.
- [39] a) K. D. Demadis, C. M. Hartshorn, T. J. Meyer, *Chem. Rev.* **2001**, *101*, 2655–2685; b) J.-P. Launay, *Chem. Soc. Rev.* **2001**, *30*, 386–397; c) M. H. Chisholm, B. J. Lear, *Chem. Soc. Rev.* **2011**, *40*, 5254–5265.
- [40] A. B. Wragg, S. Derossi, T. L. Easun, M. W. George, X.-Z. Sun, F. Hartl, A. H. Shelton, A. J. H. M. Meijer, M. D. Ward, *Dalton Trans.* **2012**, *41*, 10354–10371.
- [41] D. M. D'Alessandro, F. R. Keene, *Chem. Soc. Rev.* **2006**, *35*, 424–440.

Received: March 27, 2013

Revised: April 13, 2013

Published online: June 14, 2013